Journal of Petroleum Science and Engineering 218 (2022) 110973

Contents lists available at ScienceDirect

Journal of Petroleum Science and Engineering

journal homepage: www.elsevier.com/locate/petrol

Effects of different types of fractures on shale gas preservation in Lower Cambrian shale of northern Sichuan Basin: Evidence from macro-fracture characteristics and microchemical analysis

He Tian [a,b], Lianbo Zeng [a,b,*], Shijie Ma [a,b], Hong Li [c,f], Zhe Mao [a,b], Yongmin Peng [d], Xiang Xu [b,e], Dongjun Feng [d]

[a] State Key Laboratory of Petroleum Resources and Prospecting, China Petroleum University(Beijing), Beijing, 102249, China
[b] College of Geosciences, China University of Petroleum(Beijing), Beijing, 102249, China
[c] Geological Exploration & Development Research Institute CNPC Chuanqing Drilling Engineering Co., Ltd., Chengdu, Sichuan, 610051, China
[d] Sinopec Petroleum Exploration and Development Research Institute Co., Ltd, Beijing, 100083, China
[e] Hunan Earthquake Agency, Changsha, 410004, China
[f] CCDC Sulige Project Managment Department, Erdos, Inner Mongolia, 017000, China

ARTICLE INFO

Keywords:
Natural fracture
Qiongzhusi Formation
Shale
Rare earth elements
Shale gas preservation

ABSTRACT

The Lower Cambrian Qiongzhusi shale is the main producing layer of shale gas in the northern Sichuan Basin. Natural fractures are considered an important factor that influences the exploration and development of shale gas. In this study, outcrops, drill cores, thin sections, fluid inclusions and rare earth element (REE) were analyzed to determine the characteristics, changes in fluid chemistry, and fluid source of different types of fractures and then reveal their effects on the accumulation and preservation of shale gas. Natural fractures of Qiongzhusi shale are mainly composed of non-strata-bounded fractures (NSBFs), strata-bounded fractures (SBFs), and bed-parallel fractures (BPFs). NSBFs span multiple layers, which can significantly enhance the vertical connectivity of shale reservoirs. There are three dominant orientations of NSBFs, as N-S, NNE-SSW, and E-W trends. The E-W trending fractures, which intersect with the maximum principal stress (NWW-SEE) at a small angle, have larger permeability and control the vertical leakage of shale gas. SBFs are confined to individual layers. Homogenization temperatures of aqueous inclusions in SBF veins vary from 149.7 to 172.3 °C. Calcite veins exhibit positive Eu anomalies (δEu = 11.71, 27.9). Analysis of fluid inclusions and rare earth elements indicated that SBF vein-precipitating fluids were derived from the surrounding wall rock. The development of SBFs contributes to shale gas enrichment. BPFs are parallel to bedding planes or intersect at a low angle (<20°). Microstructural analysis suggests that cemented BPFs form from the multiple crack-seal processes. The temperature of fluid during mineral precipitation exceeds 200 °C. REE concentrations vary significantly across the BPF veins (δEu = 2.31–119.37), donating that fluid characteristics episodically changed during vein growth. The methane inclusions trapped in cements and mixing externally sourced fluids indicate that BPFs are the preferential fluid-flow pathway of shale gas and controls the lateral migration of shale gas.

1. Introduction

As clean energy, shale gas is characterized by large reserves, wide distribution, and has been attached of great importance to all countries in the world (Stevens, 2012; Wang et al., 2014; Zou et al., 2021). In 2018, the shale gas production of the United States reached 6669 × 10^8 m^3, which accounted for 63.4% of the total natural gas production (Jiang et al., 2020) and changed the global natural gas supply pattern. Sichuan Basin is the main area for shale gas exploration and development in China, which has built several shale gas fields with proven geological reserves of more than 100 billion cubic meters, such as Changning, Weiyuan, Zhaotong, Fuling, and Rongxian. (Guo, 2014; Wang, 2014; Liang et al., 2016; Liu and Wang, 2016; Ma and Xie, 2018; Jiang et al., 2020; Tian et al., 2021). The lower Cambrian Qiongzhusi shale is one of the best hydrocarbon source rocks in Sichuan Basin, dominated by black or gray-black mud shale, with wide distribution,

* Corresponding author. State Key Laboratory of Petroleum Resources and Prospecting, China Petroleum University(Beijing), Beijing, 102249, China.
E-mail address: lbzeng@sina.com (L. Zeng).

https://doi.org/10.1016/j.petrol.2022.110973
Received 28 November 2021; Received in revised form 26 July 2022; Accepted 12 August 2022
Available online 17 August 2022
0920-4105/

high TOC content, good organic matter type and high maturity, which is the chief formation for shale gas exploration and development in next step (Cao et al., 2011; Liu et al., 2017; Zhao et al., 2019). Natural fractures can enhance storage capacity and permeability for shale gas reservoirs, which are the main channels for shale gas migration and have a significant effect on shale gas preservation (Curtis, 2002; Gale et al., 2014; Zeng et al., 2016; Tian et al., 2020; Xu et al., 2021). However, the development characteristics of different types of fractures vary greatly, which caused their influence on shale gas production is still controversial. Veins are common features of fractures and record the information on metamorphic conditions, fluid characteristics, and fluid origin during fracture formation (Bons, 2000; Barker et al., 2006; Wagner et al., 2010; Bons et al., 2012; Evans et al., 2012), which can reflect the enrichment and preservation conditions of shale gas (He et al., 2016; Teixeira et al., 2017; Lei et al., 2018; Zhang et al., 2019; Tian et al., 2020).

In this study, we integrated macro-characteristics and microchemical analysis of different types of fractures to clarify their effects on shale gas preservation in the Qiongzhusi shale. The large-scale NSBFs characteristics and their influences on shale gas production were analyzed based on the outcrop observation and in-situ stress analysis. Microstructural observations, fluid inclusions, and in-situ rare earth element analyses are used to determine variations of fluid chemistry in SBFs and BPFs, and then reveal their fluid sources and effects on shale gas preservation.

2. Geological setting

Nanjiang area is located in the north of the Upper Yangtze block, which is bounded by the Micang mountain, Daba mountain, and Longmenshan Fault in the north, East and west, respectively (Fan et al., 2011). The study area is a monocline structure, which is mainly controlled by three sets of detachment layers of Presinian, Sinian, and Triassic, and the structural strength decreases from north to south (Fig. 1) (Zhu et al., 2013; Li et al., 2018). Qiongzhusi Formation can be divided into lower, middle, and upper members. The lower member is composed of black carbonaceous shale, sandy shale, and argillaceous siltstone (Fig. 2). The middle member mainly consists of sandy shale, silty limestone and siltstone. The upper member is characterized by gray calcareous siltstone interbedded, with increased calcareous content. The total organic carbon (TOC) content in Qiongzhusi shale ranges from 0.19% to 10.66%, and the organic matter type is mainly type I. The thermal maturity is between high maturity and over maturity. Organic matters are in the high and ultra-mature stage. Qiongzhusi shale is primarily composed of high content of quartz, clay, feldspar, and low content of calcite (less than 10%). The quartz content is 30%–54%, with an average of 38%; The clay minerals content ranges from 9% to 38%, with an average of 25%. The porosity and permeability in Qiongzhusi shale are 2.10%–7.14% and 0.0015 × 10^{-3}μm^2 to 0.009 × 10^{-3}μm^2, respectively (Shan, 2020).

3. Data and methods

Large fracture information is difficult to obtain from cores due to the borehole diameter limitation. At the same time, bed-parallel fracture density in outcrops is usually underestimated due to weathered bedding and argillaceous fabric (Gale et al., 2014). Therefore, in this study, large NSBFs characteristics (length, dip angle, strike, and density) of Qiongzhusi shale were mainly obtained from 4 outcrops in the Northern Sichuan Basin. Limited by the trend of field sections, not every set of

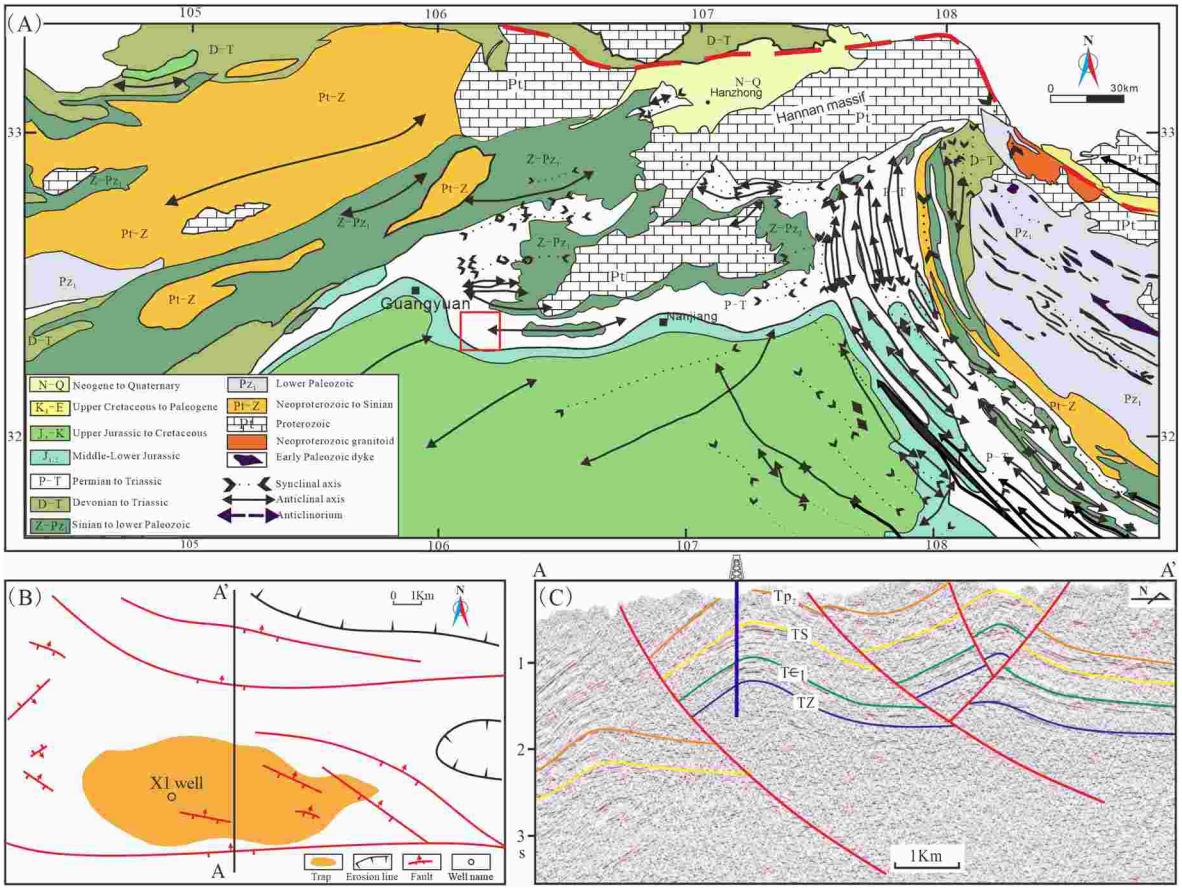

Fig. 1. (A) Surface geological map of Micangshan and its surrounding areas (adapted from Zhang et al., 2010). (B) Map showing the distributions of major faults and location of well X1. (C) Interpretation map of typical seismic profile (N-S trend) across the well X1, showing the structural pattern of the strata. (The location of the cross-section is shown by A-A′ in Fig. 1 B).

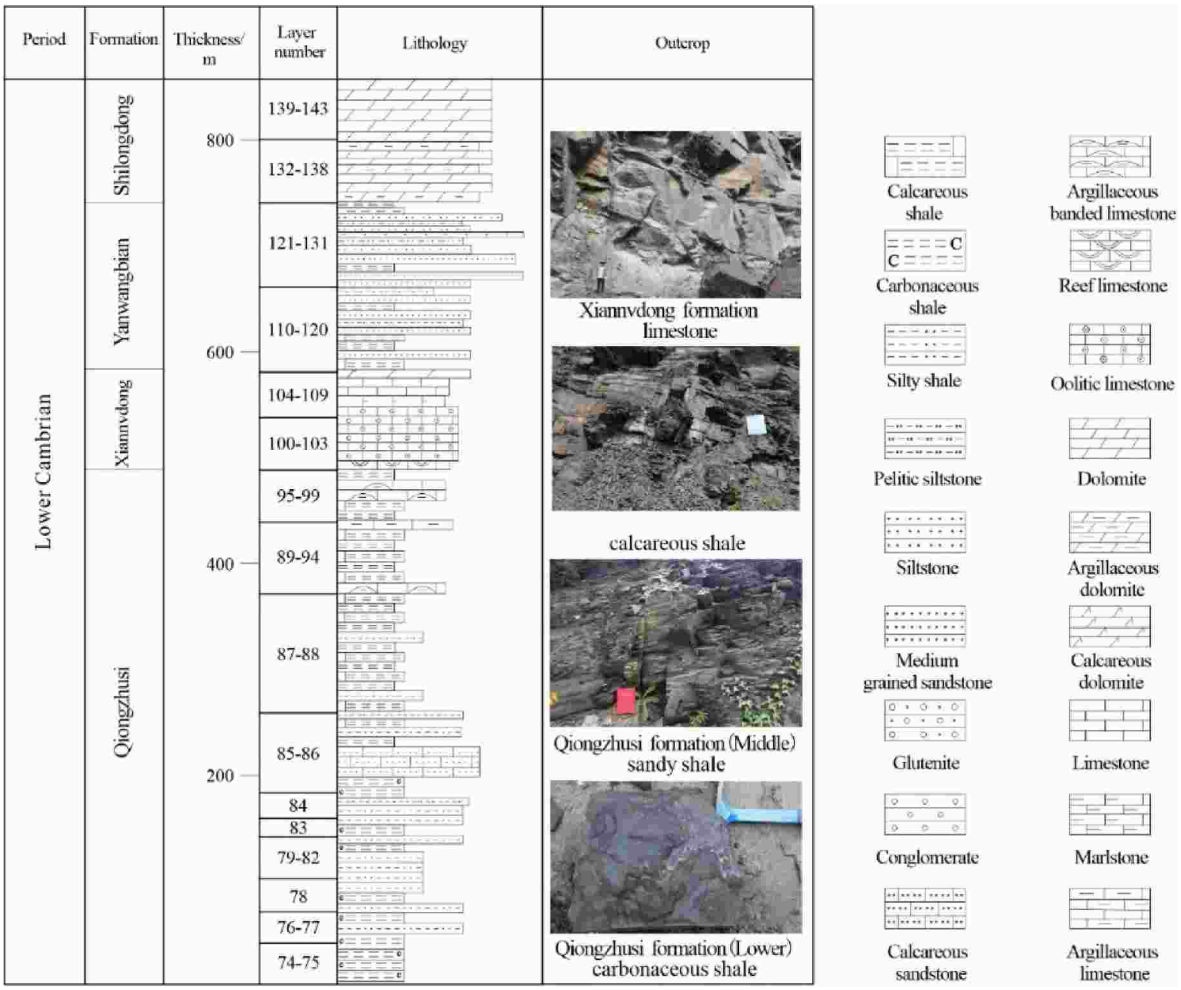

Fig. 2. Stratigraphic column of the Nanjiang area (adapted from Cao et al., 2011).

fractures can be observed in one Section. Therefore, this paper selects one set fracture (E-W) to explore the vertical variation of fracture density. The present-day horizontal maximum stress orientations (S_{Hmax}) within the Qiongzhusi Formation are mainly determined based on borehole breakouts (BOs) and drilling-induced fractures (DIFs) from well X1. BOs indicate the orientation perpendicular to S_{Hmax} (Zoback et al., 2003; Schmitt et al., 2012; Williams et al., 2015; Rajabi et al., 2016), and the orientation of DITFs are parallel to S_{Hmax} (Tingay et al., 2010; Kingdon et al., 2016; Rajabi et al., 2010, 2016).

The development characteristics SBFs and BPFs were observed from well X1. Two SBF veins and two BPF veins were collected for fluid inclusions, Raman spectral, and in situ rare earth element analyses. The detailed information on samples is shown in Table 1. Thin sections of SBFs and BPFs were analyzed using Leica microscope and CL8200-MK5 cathode luminescence instrument. Fluid inclusions petrography were observed by Leica M165C stereoscopic microscope and Zeiss Imager A2m polarizing/fluorescence microscope. Homogenization temperatures of fluid inclusions were measured by thermal cycling using temperature steps of 0.1–5 °C/min. The composition of gas inclusions was determined by Renishaw Invia laser Raman spectrometer (Renishaw, UK) with an output laser power of 5–10 mW, a beam spot size of about 1 μm, and a spectral resolution of 2 cm^{-1}. The rare earth element (REE) distribution in SBFs and BPFs was conducted in situ by LA-ICP-MS. Fractures were measured using a COMPexPro 102 ArF excimer laser (λ = 193 nm) and ICP-MS (Agilent 7900e). This study's laser spot size and frequency are 44 μm and 5 Hz, respectively. REE compositions of fracture veins were calibrated against a series of standard materials (NIST610, BHVO-2G, BIR-1G, BCR-2G, MACS-3).

4. Results

4.1. Natural fracture characteristics

4.1.1. Non-strata-bounded fractures

Non-strata-bounded fractures (NSBFs) pass through numerous layers and usually span entire outcrop (Fig. 3). Fracture heights range from

Table 1
Details of fracture veins selected from well X1 for fluid inclusion and rare earth element analysis in Nanjiang area, Northern Sichuan Basin. Samples investigated in this study include depth, stratigraphic position, fracture type, the morphology of crystals, and the mineral phase of the fracture veins.

Well name	Sample	Depth (m)	Stratigraphy	Fracture type	Morphology of crystals in veins	Dominant mineralogy of veins
X1	SBF1	1730.1	Qiongzhusi Formation	Strata-bounded fracture	Blocky	Calcite
	SBF2	1732.6	Qiongzhusi Formation	Strata-bounded fracture	Blocky	Calcite
	BPF1	1730.4	Qiongzhusi Formation	Bed-parallel fracture	Blocky	Calcite + Quartz
	BPF2	1732.9	Qiongzhusi Formation	Bed-parallel fracture	Blocky	Calcite + Quartz

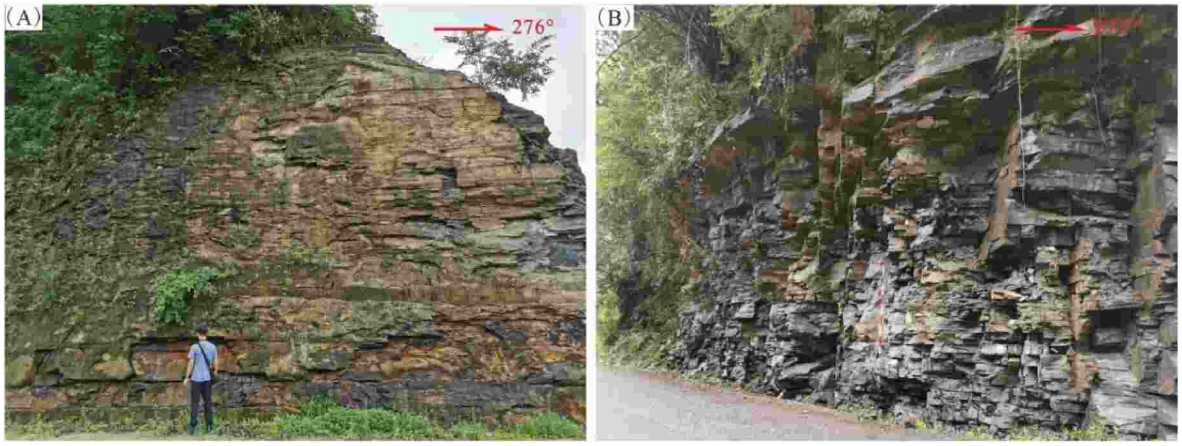

Fig. 3. Non-strata-bounded fractures (NSBFs) in outcrops. (A) West-east-striking NSBFs in Shatan outcrop. (B) South-north-striking NSBFs in Guchengxiang outcrop.

several meters to tens of meters measured in outcrops of the Nanjiang area. These fractures always have planar fracture surfaces and are at a high angle to bedding planes (>60°). Additionally, most NSBFs are unfilled in outcrops, while only a few cement-filled fractures are observed. Fractures are mainly at the N-S, NNE-SSW, and near E-W strikes (Fig. 4A–C). The average linear density of E-W trending fractures increases from the bottom to the top of Qiongzhusi shale (Fig. 4D). Core observations show that NSBFs are widespread in Qiongzhusi shale and account for 48.7% of all fractures (Fig. 5A). NSBFs heights are mainly distributed between 10 cm and 50 cm, the tallest fracture extends up to 78 cm in cores (Fig. 5B). However, most NSBFs terminate outside the core, so the fracture height measured on the core is usually lower than the true height of NSBFs. Sealed NSBFs have apertures of less than 1 mm (Fig. 5C), and fracture dip angles range from 60° to 90° (Fig. 5D).

4.1.2. *Strata-bounded fractures*

Strata-bounded fractures (SBFs) are confined to a single layer. Fracture tips terminated at the lower and upper bed boundaries (bedding planes, bed-parallel fractures) (Fig. 6A、B). SBFs constitute 19.5% of all fractures in Qiongzhusi shale (Fig. 5A). Fracture heights are

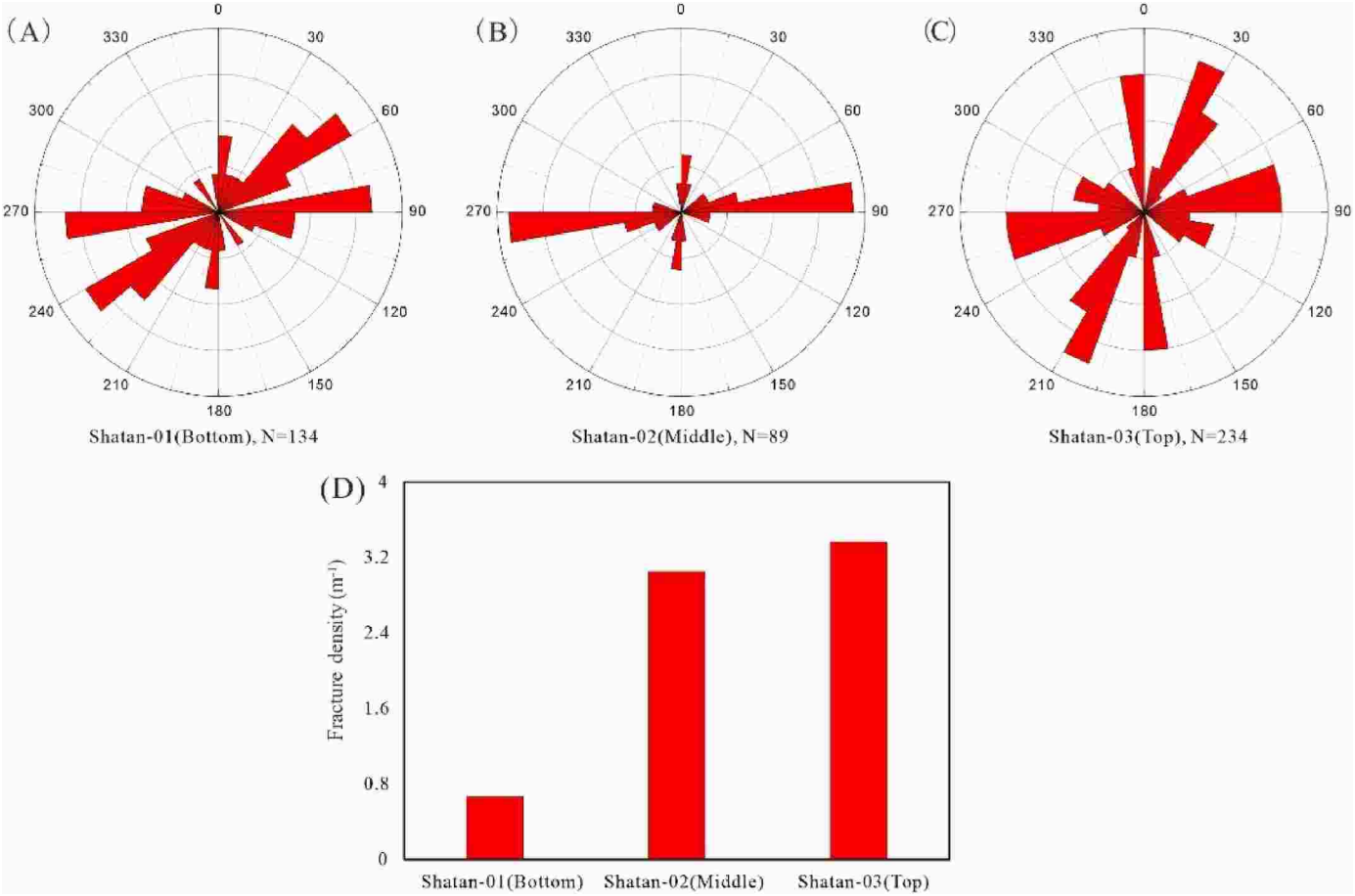

Fig. 4. Strike rose diagram of NSBFs in different outcrops in the Nanjiang area. (A) Bottom of the Qiongzhusi shale, Shatan-01. (B) Middle of the Qiongzhusi shale, Shatan-02. (C) Top of the Qiongzhusi shale, Shatan-03. (D) The average linear density of East-West trending fractures of Qiongzhusi shale in Shatan outcrops.

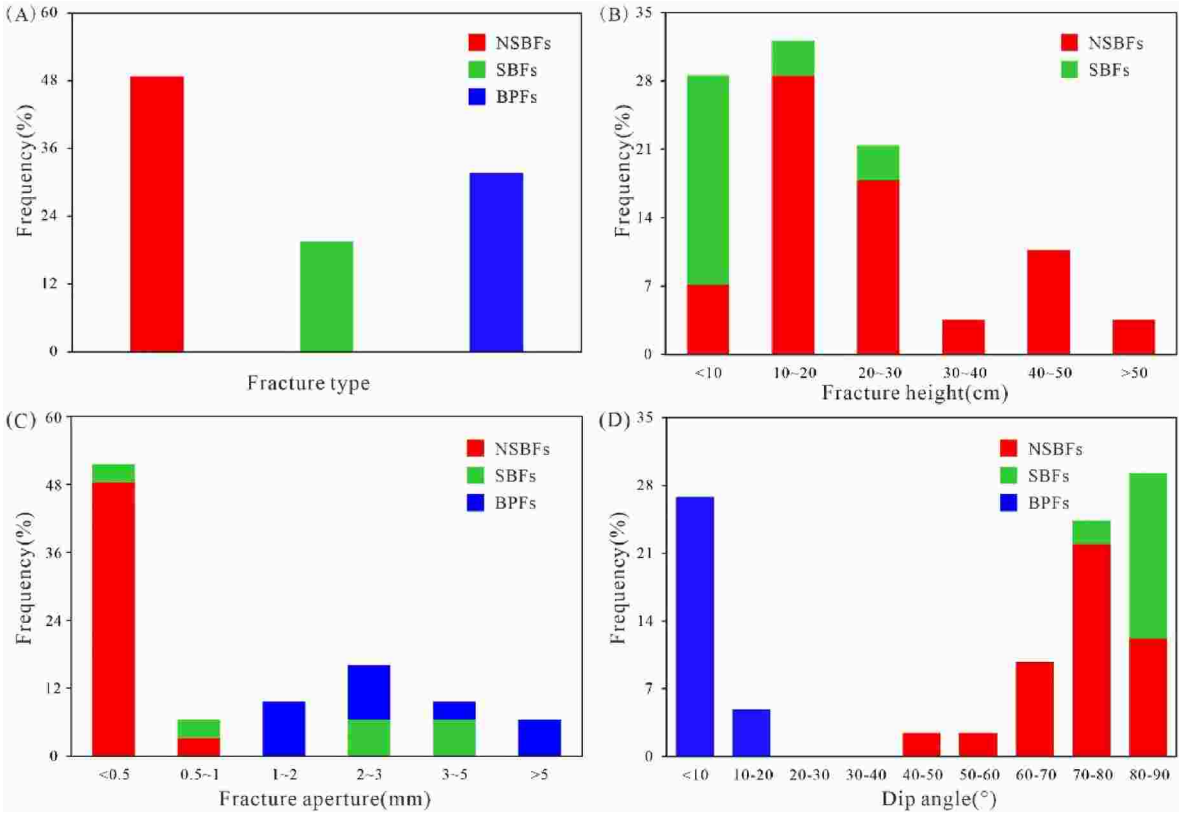

Fig. 5. Frequency distribution of the characteristic parameter for fractures in the Qiongzhusi shale. (A) The frequency distribution of the NSBFs, SBFs, and BPFs was obtained from cores. (B) Statistics of the height of fractures measured from cores. (C) Statistics of the aperture of fractures obtained from cores. (D) Statistics of the dip angle of fractures measured from cores.

controlled by bed thicknesses and range from 5 cm to 30 cm (Fig. 5B). Mineral SBFs widths range from 0.1 mm to 5 mm in cores (Fig. 5C). These fractures are commonly perpendicular to bedding planes, therefore their dip angles are mainly greater than 80° (bed dip angle is less than 10° in cores) (Fig. 5D). The fracture spacing is between 1 cm and 8 cm. Samples collected from well X1 have two types of cementations, tiny quartz crystals preserved at the margin of the SBF and the central portion are filled with larger calcite crystals (Fig. 6C). CL image shows that the calcite crystals have a brighter orange color while the quartz crystals and host rock are black (Fig. 6D).

4.1.3. Bed-parallel fractures

Bed-parallel fractures (BPFs) are parallel to bedding planes or intersect at a low angle (<20°). BPFs constitute 31.7% of all fractures in Qiongzhusi shale (Fig. 5A). Single BPFs can be traced along strike for tens of meters. Unfilled bed-parallel fracture surfaces are smooth, mirror-like, and have clear scratch traces implying a bedding parallel shear slip (Fig. 7A). Cemented fracture widths range from 3 mm to 20 mm (Fig. 5C) and the internal texture of BPF veins is characterized by crack-seal texture. BPF veins are generally composed of multiple layers of coarse-grained, blocky calcite bands, separated by thin host-rock and finer-grained quartz crystals subparallel to vein margins (Fig. 7B–E). The thickness of a single calcite strip in BPF veins is between 800 μm and 1200 μm (Fig. 7D). These microstructures are interpreted to result from the repeated opening of fracture, which is subsequently sealed by mineral precipitation (Ramsay, 1980; Laubach et al., 2004; Renard et al., 2005; Holland and Urai, 2010; Becker et al., 2011; Bons et al., 2012).

4.2. Fluid inclusion analysis

Two-phase aqueous inclusions were observed in SBF veins. The fluid inclusions observed in SBF consist of two-phase aqueous inclusions. Most of them are irregular ellipses and range from 2.3 to 4.9 μm in size (Fig. 8A and B). Measured homogenization temperatures of aqueous inclusions in SBF vary from 149.7 to 172.3 °C (Fig. 9A). No single-phase methane inclusions were found in SBFs. The observed fluid inclusions in BPFs contain two-phase aqueous inclusions and single-phase methane inclusions. Aqueous inclusions are mostly elliptical and irregular ellipses, with a size of 3–10 μm. Microthermometric analyses of aqueous inclusions homogenization temperatures (Th) in BPFs exceeds 200 °C (Fig. 9B). The single-phase methane inclusions have a relatively regular or elliptical shape and range from 5 to 10 μm in size. Methane inclusions are characterized by light in the center, dark around, and low transparency (Fig. 8C). Raman spectroscopic analyses show that the methane inclusion's Raman scatter peak v1 is 2912.07 cm^{-1}, indicating that this inclusion is pure methane inclusion (Fig. 8D).

4.3. Rare earth element chemistry of natural fractures

The REE + Y data and patterns of SBFs and BPFs are presented in Table 2 and displayed in Fig. 10. REE + Y concentrations of fractures are normalized against Post Archean Australian Shale (subscript PAAS) (McLennan, 2001). The total REE (ΣREE) concentrations of SBFs in the Qiongzhusi shale are 35.08 and 42.51 ppm. REE concentrations change significantly across the BPFs, which range from 6.01 to 174.4 ppm. Most samples are characterized by enrichment in MREE relative to LREE and HREE displayed by $(Pr/Sm)_{PAAS}<1$ and $(Tb/Yb)_{PAAS}>1$. SBF2, BPF1-1, BPF1-2, and BPF2-3 exhibit $(REE)_{PAAS}$ patterns with $(Pr/Yb)_{PAAS}>1$ that indicate enrichment in LREE relative to HREE. SBF1, BPF2-2, BPF2-4, and BPF2-5 display enrichment in HREE relative to LREE shown by $(Pr/Yb)_{PAAS}<1$. The calcite veins within the SBFs show positive Eu anomalies (δEu = 11.71, 27.90) (Fig. 10A). The REE patterns of BPF1-2 and BPF2-1 exhibit higher positive Eu anomalies (δEu = 119.37, 104.23) as compared to those within BPF1-1, BPF2(2-5) (δEu =

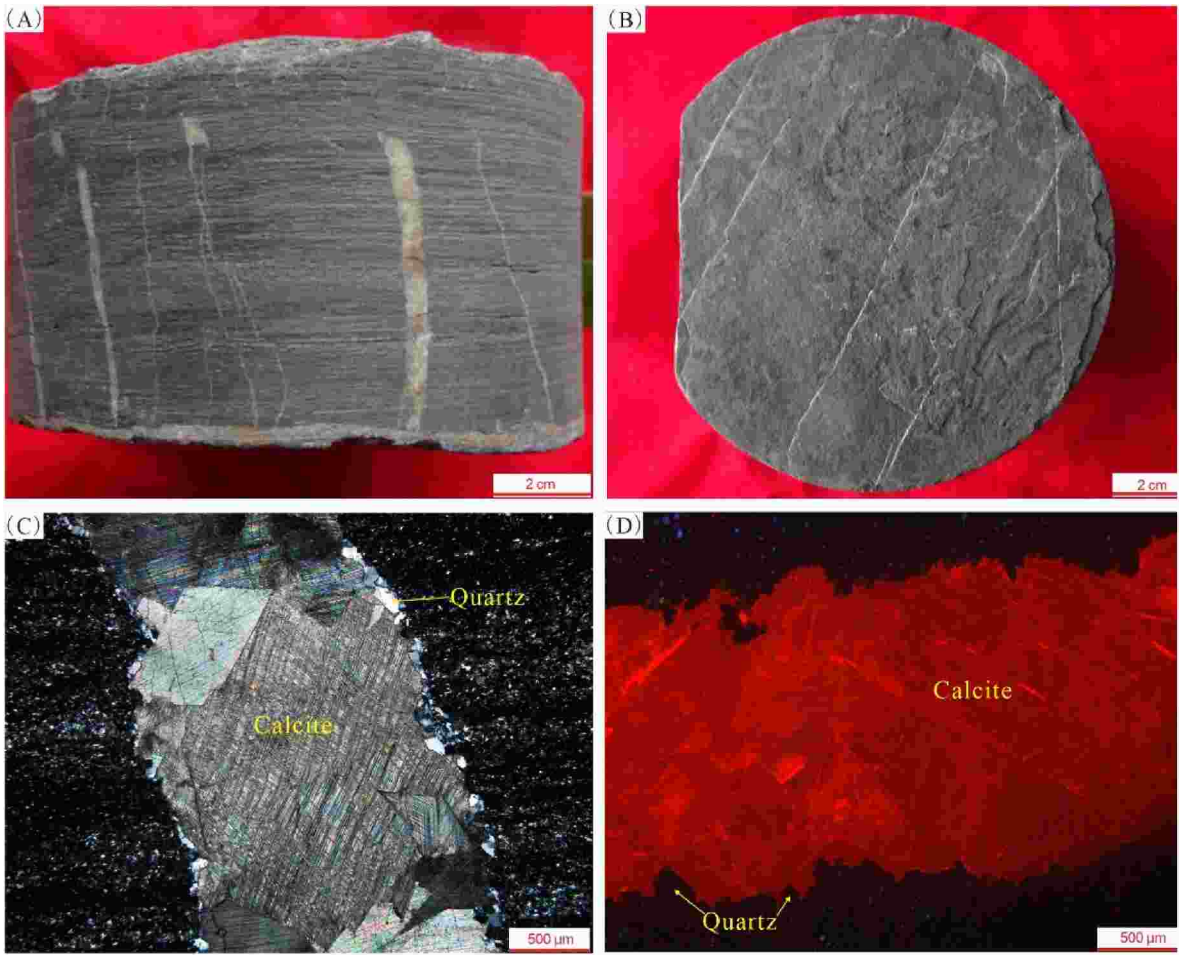

Fig. 6. Strata-bounded fractures (SBFs) in cores and thin sections (burial depth 1730.1). (A) SBFs are perpendicular to bedding planes. The top of SBFs terminates at bedding planes and the bottom terminate at bed-parallel fracture. (B) Bedding plane of SBFs termination. (C) Small quartz crystals along SBF margins with coarser calcite crystals in center. (D) Cold cathodoluminescence of SBF.

2.31–8.41) (Fig. 10B).

5. Discussion

5.1. Fluid sources of SBFs and BPFs

The concentration, distribution patterns and element anomaly of REEs in calcite veins record the information on chemistry, oxidation state and the temperature of fluid during vein formation, which is conductive to determine the source and pathway of the fluid (Dromgoole and Walter, 1990; Bau and Möller, 1992; Watson, 2004; Barker et al., 2006; Uysal et al., 2011; Bons et al., 2012; Gong et al., 2019, 2021). Previous studies suggest that the Eu^{2+}/Eu^{3+} redox increased sharply with temperature. The Eu^{2+} concentration of fluid exceeds the Eu^{3+} when the temperatures exceed 200 °C. Eu^{2+} substitutes for Ca^{2+} preferentially and results in positive Eu anomalies during the growth of veins (Sverjensky, 1984; Bau and Möller, 1992; Uysal et al., 2011). Furthermore, the host rock Eu^{2+} concentration is influenced by the content of CA-Plagioclase, in which the Eu^{2+} is much more enriched than other REEs (Lee et al., 2003; Barker et al., 2006). Consequently, changes of δEu in the minerals precipitating from a fluid are not only controlled by the fluid temperature, but also depend on the location and degree of fluid-rock reaction. Eu anomalies of veins are influenced by the temperature and Eu^{2+} concentration of the surrounding wall rocks. Microthermometric measurements of aqueous fluid inclusions in SBF veins within the Qiongzhusi shale show that the temperature of fluid during mineral precipitation is between 149.7 °C and 172.3 °C (lower than 200 °C). X-ray diffraction (XRD) analysis showed that the plagioclase content of Qiongzhusi shale ranges from 4% to 11.1%, with an average value of 8%, which indicates that plagioclase dissolution of shale can influence the Eu^{2+} composition of fluids from which vein-filling calcite precipitated. Therefore, the pronounced positive Eu anomalies in the SBF of the Qiongzhusi shale is mainly caused by the dissolution of plagioclase rather than the hydrothermal fluids. Microthermometric measurements of aqueous fluid inclusions in BPF veins exceeds 200 °C, which implies that the significantly Eu anomalies of BPFs are probably due to both precipitation temperatures (>200 °C) and the dissolution of plagioclase in host rocks. However, the positive Eu anomaly of BPF1-1, BPF2(2-5) is significantly lower than that of BPF1-2, BPF2-1, and even lower than SBFs, which are probably the result of the external fluid with lower Eu^{2+} concentration mixed into the fluids during the growth of veins, diluting the influence of temperature and the dissolution of plagioclase.

5.2. The significance of natural fractures in shale hydrocarbon reservoirs

Shale gas reservoirs are characterized by low porosity and low permeability. Natural fractures are crucial factors influencing the exploration and development of shale gas. On the one hand, natural fractures as an essential storage space of shale gas and contribute to shale gas enrichment. But on the other hand, natural fractures act as the fluid-flow pathway to enhance the permeability of shale reservoirs and destroy the preservation of shale gas (Curtis, 2002; Engelder et al., 2009; Gale and Laubach, 2009; Gale et al., 2007, 2014; Zeng et al., 2013, 2016;

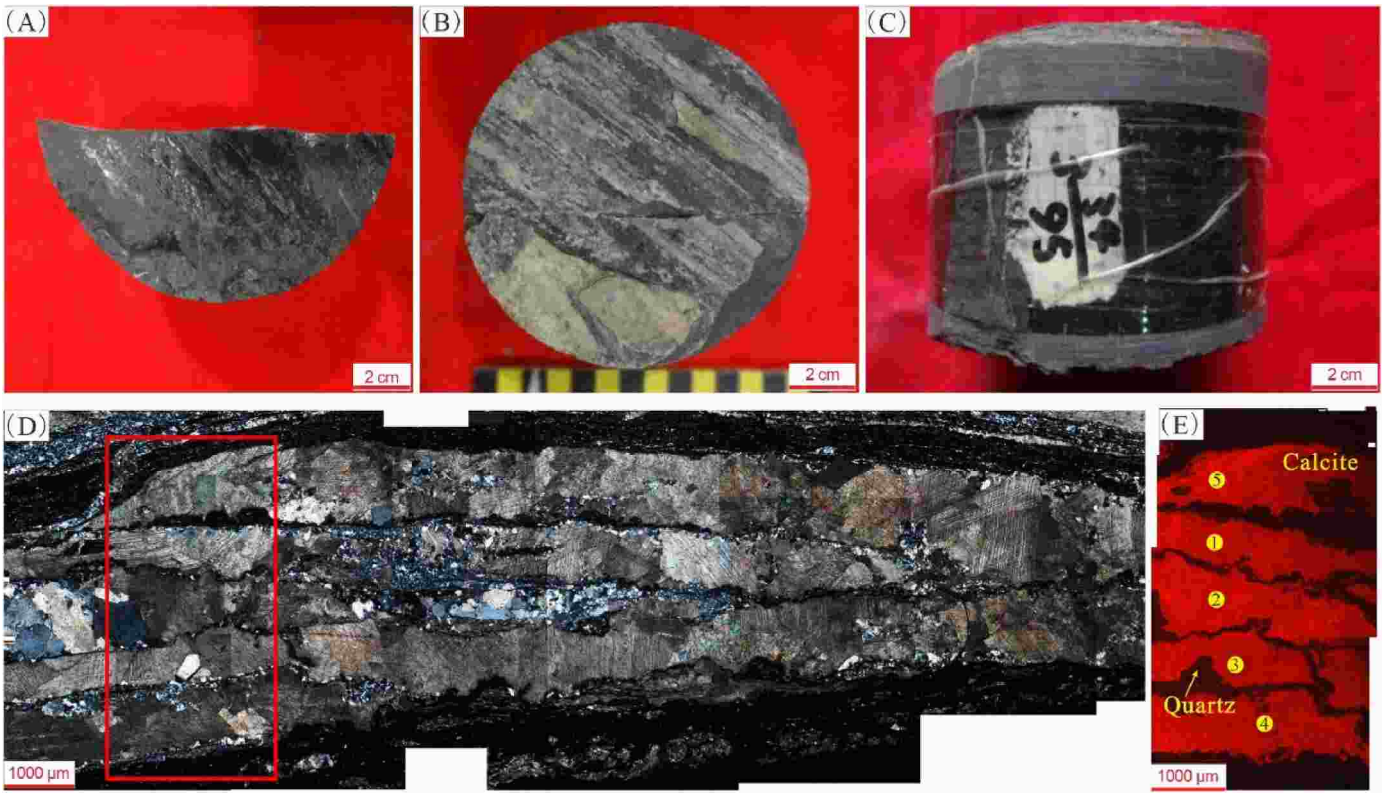

Fig. 7. Bed-parallel fractures (BPFs) in cores and thin sections. (A) Unfilled BPF with clear scratch traces. (B) and (C): Sealed BPFs in cores. (D) Crack-seal calcite vein with parallel host-rock inclusions and small quartz crystal bands that illustrate multiple crack-seal events (BPF2, burial depth, 1732.9 m). (E) Cold cathodoluminescence of SBF in (D). Holes (shown by yellow dots on the sketch) mark the locations of individual REE analyses.

Gong et al., 2021). Whether the significance might be positive or negative for shale gas production depends on the scale of fractures rather than the density (Zeng et al., 2016; Tian et al., 2020).

Natural fractures are abundant in the Qiongzhusi shale. The scales of different types of natural fractures are pretty different, resulting in their effects on shale gas preservation conditions vary greatly. Outcrop observation shows that NSBFs are characterized by large scale (several meters to tens of meters) and steeply dipping angles. These fractures cut through several mechanical layers, which can cause the cross-layer migration of shale gas and lead to the vertical loss of shale gas, and therefore destroy the vertical preservation conditions of shale gas. Fig. 11 shows that the NSBFs density decreases with the burial depth, indicating that the preservation condition at the bottom of Qiongzhusi shale is better than that at the top. As a result, the total gas content in the study area shows a decreasing trend from bottom to top (Fig. 11). Quartz, felspar, and carbonates are considered the hard minerals in shale, which control the brittleness of shale. The quartz content usually shows a positive correlation with the number of fractures (Zeng et al., 2013; Labani and Rezaee, 2015; Rybacki et al., 2016; Tian et al., 2020). In the Qiongzhusi shale, the quartz content also decreased with the burial depth (Fig. 11), probably explaining the decreased fracture density (Fig. 11). Under the compression of Micang mountain, the deformation of Qiongzhusi shale gradually increases from south to north (Figs. 1C, Fig. 2 in Zhu et al., 2013), resulting in more developed faults and fractures near Micang mountain. In addition, the horizontal compression leads to uplift and denudation of the northern strata, and shale gas is easy to dissipate along the large-scale NSBFs. Therefore, the preservation condition in the south of Qiongzhusi shale is better than that in the north.

Steeply dipping NSBFs permeability is affected by the present-day stress field, fracture transmissivities increasing with the angle between the fracture orientation and the present-day maximum compressive stress decreasing (Finkbeiner et al., 1997; Bell, 2006; Mattila and Tammisto, 2012; Ju et al., 2018; Ju and Wang, 2018). BOs and DIFs from borehole imaging logs show that the orientation of the S_{Hmax} in Nanjiang area is NWW-SEE strike (Fig. 12A–C). For the three groups of NSBFs in the study area, nearly E-W trending fractures are at small angles (20°–30°) to S_{Hmax} (Fig. 12D), and fractures in N-S and NNE-SSW are oblique to the S_{Hmax} orientation with large angles (60°–90°). Consequently, nearly E-W striking fractures have larger permeability and control the preservation of shale gas in the Nanjiang area.

The scales of SBFs are small (5–30 cm), and fractures are mainly developed in the layer. Furthermore, analysis of inclusions and REEs shows that the vein-forming material of SBFs is derived from the surrounding wall rock. Fluid transports through these fractures at a short distance, which cannot damage the storage conditions of shale gas. Besides, open SBFs can provide storage space for shale gas, which contributes to shale gas enrichment. Bed-parallel fractures have a large scale, extending for tens of meters along the bedding plane in the outcrop. Sealed BPFs generally contain many host-rock inclusion trails, denoting many crack-seal events occurred during BPF veins formation. The large width (0.8–1.2 mm) of the individual calcite band indicates it takes a long time to seal after the fracture opens. The methane inclusions trapped in the cement suggest that BPFs were formed during shale gas generation, and BPFs are the lateral migration channel of shale gas; Furthermore, the difference in REE patterns in BPFs suggests that fluid chemistry episodically changed during vein growth (Figs. 10B and 13). The mixing of externally sourced fluids indicates that shale gas can transport a long distance through BPFs. Taken together, BPFs are the key factor in controlling the lateral migration of shale gas.

6. Conclusion

Natural fractures of Qiongzhusi shale in the northern Sichuan Basin

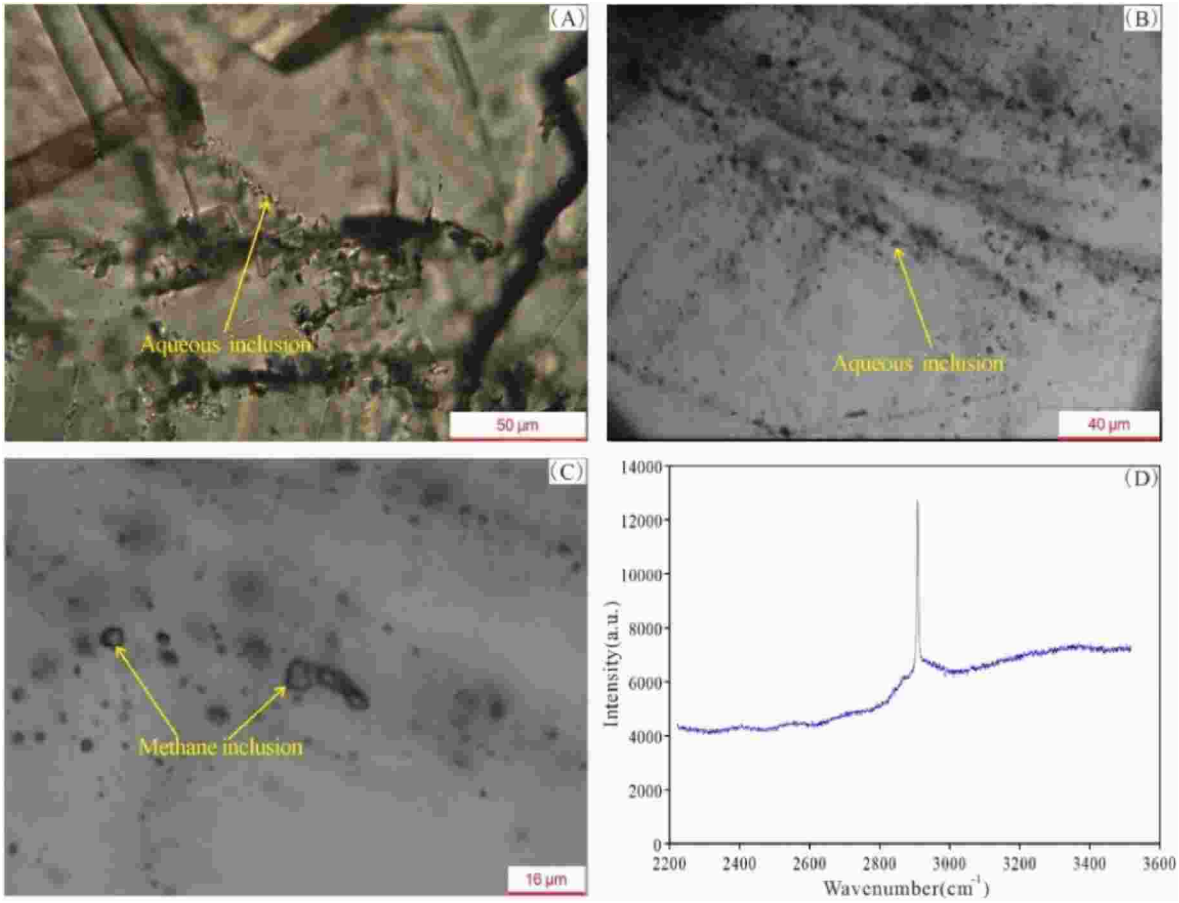

Fig. 8. (A) Representative aqueous inclusions were trapped in veins from SBF (Qiongzhusi Formation, measured depth 1730.1 m). (B) Representative aqueous inclusions were trapped in veins from BPF2 (Qiongzhusi Formation, measured depth 1732.9 m). (C) Methane inclusions were trapped in veins from BPF2. (D) Laser Raman spectra were collected from pure methane inclusions "Fig. 8C".

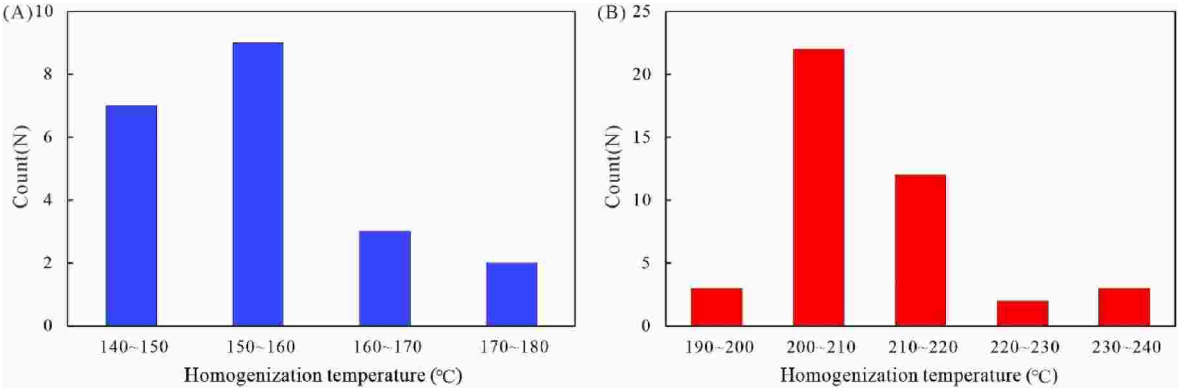

Fig. 9. Homogenization temperature (Th) histograms of aqueous inclusions in the SBFs (A) and BPFs (B).

are mainly composed of non-strata-bounded fractures (NSBFs), strata-bounded fractures (SBFs), and bed-parallel fractures (BPFs).

NSBFs span multiple layers, and fracture heights range from several meters to tens of meters in outcrops. There are three dominant orientations of NSBFs, N-S, NNE-SSW, and E-W trends. The E-W trending fractures, which intersect with the maximum principal stress (NWW-SEE) at a small angle, have larger permeability and control the vertical leakage of shale gas in the Nanjiang area.

SBFs are confined to individual layer with fracture heights ranging from 5 cm to 30 cm and fracture widths between 0.1 mm and 5 mm in cores. Homogenization temperatures of aqueous inclusions in SBF veins vary from 149.7 °C to 172.3 °C. Calcite veins exhibit positive Eu anomalies (δEu = 11.71, 27.90). Analysis of fluid inclusions and REEs suggested that SBF vein-precipitating fluids within the Qiongzhusi shale were derived from the host rock. The development of open SBFs contributes to shale gas enrichment.

BPFs in Qiongzhusi shale are parallel to bedding planes or intersect at a low angle (<20°). BPF calcite veins with parallel host-rock inclusions and small quartz crystal bands indicate that cemented BPFs form from multiple crack-seal events. Homogenization temperatures of the aqueous inclusions in BPFs exceed 200 °C. REE concentrations vary significantly across the BPF veins (δEu = 2.31–119.37), indicating that

Table 2
REE concentrations (ppm) and related REE parameters of fracture veins from well X1 in Qiongzhusi shale of the Nanjiang area. Analysis points of BPF2 are shown in Fig. 7E.

Spot	SBF1	SBF2	BPF1-1	BPF1-2	BPF2-1	BPF2-2	BPF2-3	BPF2-4	BPF2-5
La	4.05	2.03	10.7	1.83	0.85	22.25	31.28	10.65	28.07
Ce	9.30	8.29	26.1	3.86	1.21	57.14	47.06	21.60	61.40
Pr	1.33	1.65	3.31	0.43	0.15	7.59	4.35	2.77	7.01
Nd	6.03	9.55	15.4	1.91	0.69	33.75	16.23	11.86	27.83
Sm	1.94	2.63	4.50	0.19	0.13	10.84	2.89	3.24	7.70
Eu	5.17	12.81	5.74	6.21	2.70	5.61	2.22	5.57	5.95
Gd	2.04	3.01	4.36	0.65	0.16	13.12	2.45	2.77	9.04
Tb	0.43	0.27	0.65	0.072	0.02	2.29	0.29	0.52	1.42
Dy	2.23	1.53	3.05	0.13	0.07	10.44	1.40	2.58	6.72
Y	13.24	6.80	0.52	0.042	0.43	66.61	9.67	20.07	47.53
Ho	0.45	0.16	18.97	1.67	0.01	2.08	0.21	0.61	1.42
Er	0.95	0.37	1.15	0.025	0.01	4.47	0.48	1.26	3.04
Tm	0.18	0.03	0.13	0.026	–	0.60	0.06	0.23	0.41
Yb	0.81	0.17	0.81	0.039	–	3.83	0.25	1.43	2.61
Lu	0.15	0.03	0.043	0.0077	–	0.41	0.02	0.16	0.27
ΣREE	35.08	42.51	76.44	15.41	6.00	174.40	109.17	65.24	162.91
δEu	11.71	27.90	6.48	119.37	104.24	2.31	4.42	8.41	3.61
$(Pr/Sm)_{PAAS}$	0.43	0.39	0.46	1.39	0.72	0.44	0.95	0.54	0.57
$(Tb/Yb)_{PAAS}$	1.95	5.72	2.92	6.77	–	2.18	4.17	1.34	1.99
$(Pr/Yb)_{PAAS}$	0.52	3.11	1.31	3.51	–	0.63	5.55	0.62	0.86

Note: $\delta Eu = Eu_{SN}/((Sm_{SN}^2 \times Td_{SN})^{1/3})$, where SN-normalized to PAAS (Post-Archean Australian Shale).

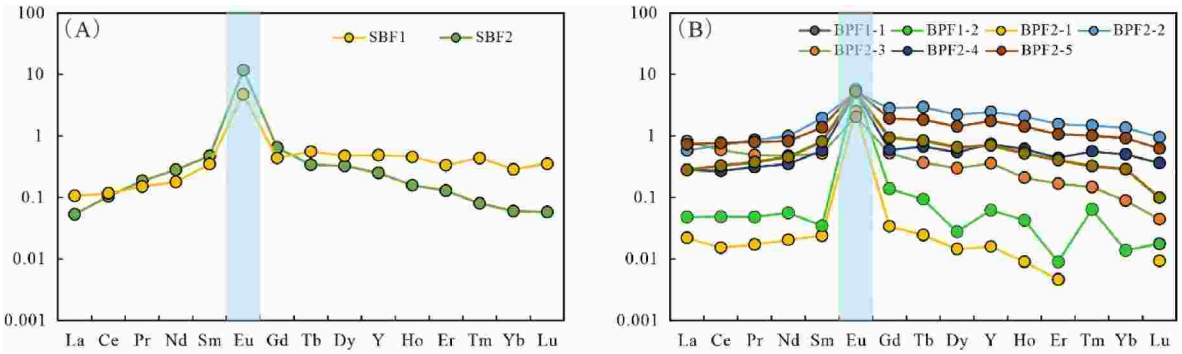

Fig. 10. (A) PAAS-normalized (McLennan, 2001) REE pattern of SBFs. (B) PAAS-normalized REE patterns of different positions in BPFs (Samples information is shown in Table 1, Fig. 7E).

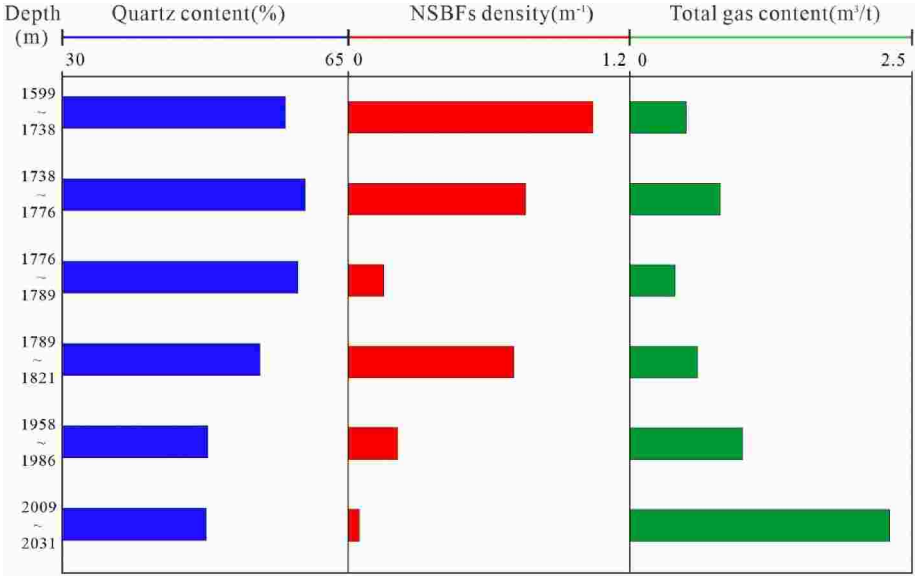

Fig. 11. (A) Variation of average quartz content, NSBFs density and total gas content with burial depth in Qiongzhusi of well X1. The quartz content was obtained from Elemental Capture Spectroscopy. The density of NSBFs was obtained from image logs.

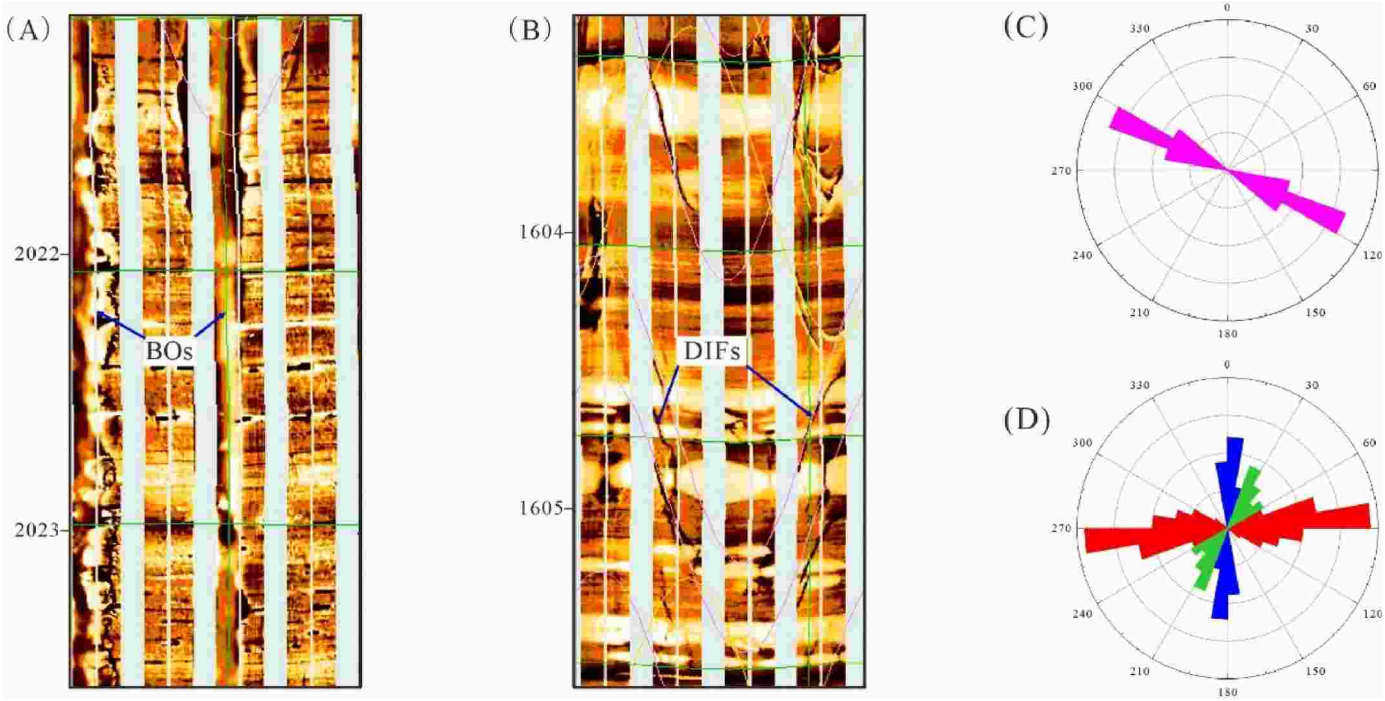

Fig. 12. Characteristics of borehole breakouts (A) and drilling-induced fractures (B) in Qiongzhusi shale interpreted from image logs. (C) Orientations of S_{Hmax} in the Qiongzhusi shale were interpreted from image logs (BOs and DIFs) (n = 178). (D) Strike rose diagram of NSBFs in the Qiongzhusi shale of Nanjiang area from Shatan Outcrops (n = 457).

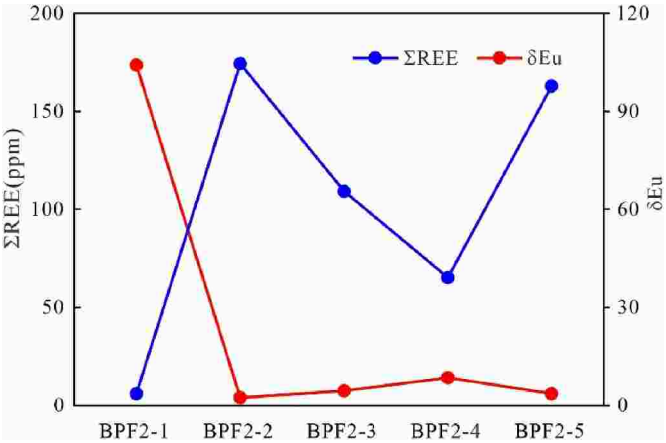

Fig. 13. Variation of ΣREE and δEu of BPF2 in Qiongzhusi shale.

fluid chemistry changed during vein growth episodically. The methane inclusions trapped in cement and mixing external fluids reveal that BPFs are the preferential fluid-flow pathway, and shale gas can transport a long distance along the bed plane. Consequently, BPFs are critical in controlling shale gas's lateral migration.

Credit author statement

He Tian contributed to outcrops, drill cores, thin sections observation, and wrote the manuscript; ***Lianbo Zeng*** provided the idea of the method and outline of the manuscript; ***Shijie Ma*** contributed to imaging logs analyses and ideas of this manuscript; ***Hong Li*** contributed to data analyses and editing of this manuscript; ***Zhe Mao*** contributed to drawing pictures, stress analysis, and checking the results; ***Yongmin Peng*** contributed to the REE testing and analysis; ***Xiang Xu*** contributed to fluid inclusions testing and analysis; ***Dongjun Feng*** contributed ideas and checked the results.

Declaration of competing interest

The authors declare that they have no known competing financial interests or personal relationships that could have appeared to influence the work reported in this paper.

Data availability

The data that has been used is confidential.

Acknowledgments

This study was financially supported by the National Natural Science Foundation of China (Grant No. U1663203), (Grant No. 33550000-19-ZC0613-0097), China Scholarship Council (CSC; grant nr. 202006440101).

References

Barker, S.L.L., Cox, S.F., Eggins, S.M., Gagan, M.K., 2006. Microchemical evidence for episodic growth of antitaxial veins during fracture-controlled fluid flow. Earth Planet Sci. Lett. 250, 331–344. https://doi.org/10.1016/j.epsl.2006.07.051.

Bau, M., Möller, P., 1992. Rare earth element fractionation in metamorphogenic hydrothermal calcite, magnesite and siderite. Mineral. Petrol. 45, 231–246. https://doi.org/10.1007/BF01163114.

Becker, S., Hilgers, C., Kukla, P.A., Urai, J.L., 2011. Crack-seal microstructure evolution in bi-mineralic quartz-chlorite veins in shales and siltstones from the RWTH-1 well, Aachen, Germany. J. Struct. Geol. 33, 676–689. https://doi.org/10.1016/j.jsg.2011.01.001.

Bell, J.S., 2006. In-situ stress and coal bed methane potential in Western Canada. Bull. Can. Petrol. Geol. 54, 197–220. https://doi.org/10.2113/gscpgbull.54.3.197.

Bons, P.D., 2000. The formation of veins and their microstructures. J. Virtual Explor. 2 https://doi.org/10.3809/jvirtex.2000.00007.

Bons, P.D., Elburg, M.A., Gomez-Rivas, E., 2012. A review of the formation of tectonic veins and their microstructures. J. Struct. Geol. 43, 33–62. https://doi.org/10.1016/j.jsg.2012.07.005.

Cao, T., Xu, S., Wang, Y., Zhou, L., Wu, X., 2011. Geobiological conditions for the Formation of the lower Cambrian source rocks in Yangba area of Nanjiang county in the Sichuan Basin. Oil Gas Geol. 32, 11–16.
Curtis, J.B., 2002. Fractured shale-gas systems. Am. Assoc. Petrol. Geol. Bull. 86, 1921–1938.
Dromgoole, E.L., Walter, L.M., 1990. Iron and manganese incorporation into calcite: effects of growth kinetics, temperature and solution chemistry. Chem. Geol. 81, 311–336. https://doi.org/10.1016/0009-2541(90)90053-A.
Engelder, T., Lash, G.G., Uzcátegui, R.S., 2009. Joint sets that enhance production from middle and upper Devonian gas shales of the Appalachian basin. Am. Assoc. Petrol. Geol. Bull. 93 (7), 857–889. https://doi.org/10.1306/03230908032.
Evans, M.A., Bebout, G.E., Brown, C.H., 2012. Changing fluid conditions during folding: an example from the central Appalachians. Tectonophysics 576–577, 99–115. https://doi.org/10.1016/j.tecto.2012.03.002.
Fan, C., Qin, Q., Zhao, L., Tang, W., Yang, Y., Li, W., 2011. Fracture development pattern of Nanjiang area. Fault-Block Oil Gas Field 18, 442–444.
Finkbeiner, T., Barton, C.A., Zoback, M.D., 1997. Relationships among in-situ stress, fractures and faults, and fluid flow: monterey formation, Santa Maria Basin, California. Am. Assoc. Petrol. Geol. Bull. 81, 1975–1999. https://doi.org/10.1306/3b05c6fe-172a-11d7-8645000102c1865d.
Gale, J.F.W., Laubach, S.E., 2009. Natural fractures in the New Albany Shale and their importance for shale-gas production. In: Int. Coalbed Shale Gas Symp. Forum, Tuscaloosa, pp. 1131–1140.
Gale, J.F.W., Laubach, S.E., Olson, J.E., Eichhubl, P., Fall, A., 2014. Natural fractures in shale: a review and new observations. Am. Assoc. Petrol. Geol. Bull. 98 (10), 2165–2216. https://doi.org/10.1306/08121413151.
Gale, J.F.W., Reed, R.M., Holder, J., 2007. Natural fractures in the Barnett Shale and their importance for hydraulic fracture treatments. Am. Assoc. Petrol. Geol. Bull. 91 (4), 603–622. https://doi.org/10.1306/11010606061.
Gong, L., Fu, X., Wang, Z., Gao, S., Jabbari, H., Yue, W., Liu, B., 2019. A new approach for characterization and prediction of natural fracture occurrence in tight oil sandstones with intense anisotropy. Am. Assoc. Pet. Geol. Bull. https://doi.org/10.1306/12131818054.
Gong, L., Wang, J., Gao, S., Fu, X., Liu, B., Miao, F., Zhou, X., Meng, Q., 2021. Characterization, controlling factors and evolution of fracture effectiveness in shale oil reservoirs. J. Pet. Sci. Eng. https://doi.org/10.1016/j.petrol.2021.108655.
Guo, X., 2014. Rules of two-factor enrichment for marine shale gas in southern China-understanding from the longmaxi formation shale gas in sichuan basin and its surrounding area. Acta Geol. Sin. 88, 1209–1218.
He, Z., Nie, H., Zhang, Y., 2016. The main factors of shale gas enrichment of Ordocician wufeng formation-silurian longmaxi formation in the sichuan basin and its adjacent areas. Earth Sci. Front. Univ. Geosci. 23, 8–17.
Holland, M., Urai, J.L., 2010. Evolution of anastomosing crack-seal vein networks in limestones: insight from an exhumed high-pressure cell, Jabal Shams, Oman Mountains. J. Struct. Geol. 32, 1279–1290. https://doi.org/10.1016/j.jsg.2009.04.011.
Jiang, Z., Song, Y., Tang, X., Li, Z., Wang, X., Wang, G., Xue, Z., Li, X., Zhang, K., Chang, J., Qiu, H., 2020. Controlling factors of marine shale gas differential enrichment in southern China. Petroleum Explor. Dev. 47 (3), 617–628.
Ju, W., Wang, K., 2018. A preliminary study of the present-day in-situ stress state in the Ahe tight gas reservoir, Dibei Gasfield, Kuqa Depression. Mar. Petrol. Geol. 96, 154–165. https://doi.org/10.1016/j.marpetgeo.2018.05.036.
Ju, W., Wang, K., Hou, G., Sun, W., Yu, X., 2018. Prediction of natural fractures in the lower Jurassic Ahe formation of the Dibei Gasfield, Kuqa Depression, Tarim basin, NW China. Geosci. J. 22, 241–252. https://doi.org/10.1007/s12303-017-0039-z.
Kingdon, A., Fellgett, M.W., Williams, J.D.O., 2016. Use of borehole imaging to improve understanding of the in-situ stress orientation of Central and Northern England and its implications for unconventional hydrocarbon resources. Mar. Petrol. Geol. 73, 1–20. https://doi.org/10.1016/J.MARPETGEO.2016.02.012.
Labani, M.M., Rezaee, R., 2015. The importance of geochemical parameters and shale composition on rock mechanical properties of gas shale reservoirs: a case study from the Kockatea shale and Carynginia formation from the Perth basin, western Australia. Rock Mech. Rock Eng. 48, 1249–1257. https://doi.org/10.1007/s00603-014-0617-6.
Laubach, S.E., Reed, R.M., Olson, J.E., Lander, R.H., Bonnell, L.M., 2004. Coevolution of crack-seal texture and fracture porosity in sedimentary rocks: cathodoluminescence observations of regional fractures. J. Struct. Geol. 26, 967–982. https://doi.org/10.1016/j.jsg.2003.08.019.
Lee, S.G., Lee, D.H., Kim, Y., Chae, B.G., Kim, W.Y., Woo, N.C., 2003. Rare earth elements as indicators of groundwater environment changes in a fractured rock system: evidence from fracture-filling calcite. Appl. Geochem. 18, 135–143. https://doi.org/10.1016/S0883-2927(02)00071-9.
Lei, J., Bin, D., Shugen, L., Yuehao, Y., Bo, S., Di, Y., Xiao, L., Rui, H., Dong, L., Yu, H., 2018. The paleo-fluid migration and conservation conditions of shale gas in the Jiaoshiba-Wulong area. Earth Sci. 44, 524–538.
Li, S., Sun, D., Cai, L., Gao, P., Li, T., Yuan, Y., Zheng, M., Qiu, D., 2018. Detrital Zircon U-Pb geochronology of Micang mountain Piedmont zone, northern Sichuan Basin and its significance to basin-mountain evolution. Geotect. Metallogenia 42, 1087–1107. https://doi.org/10.16539/j.ddgzyckx.2018.06.011.
Liang, X., Wang, G., Xu, Z., Zhang, J., Chen, Z., Xian, C., Lu, H., Liu, C., Zhao, C., Xiong, S., 2016. Comprehensive evaluation technology for shale gas sweet spots in the complex marine mountains, South China: a case study from Zhaotong national shale gas demonstration zone. Nat. Gas. Ind. B. 36 (1), 33–42. https://doi.org/10.1016/j.ngib.2016.02.003.
Liu, N., Wang, G., 2016. Shale gas sweet spot identification and precise geo-steering drilling in Weiyuan Block of Sichuan Basin, SW China. Petrol. Explor. Dev. https://doi.org/10.1016/S1876-3804(16)30124-0.
Liu, Z., Feng, D., Gao, B., Li, H., Nie, H., 2017. Micropore characteristics of high thermal evolution shale in the lower Cambrian series in Upper Yangtze area. Nat. Gas Geosci. 28, 1096–1107.
Ma, X., Xie, J., 2018. The progress and prospects of shale gas exploration and development in southern Sichuan Basin, SW China. Petrol. Explor. Dev. 38 (10), 1–10. https://doi.org/10.1016/S1876-3804(18)30018-1.
Mattila, J., Tammisto, E., 2012. Stress-controlled fluid flow in fractures at the site of a potential nuclear waste repository, Finland. Geol. 40, 299–302. https://doi.org/10.1130/G32832.1.
McLennan, S.M., 2001. Relationships between the trace element composition of sedimentary rocks and upper continental crust. Geochem. Geophys. Geosyst. 2, 1021–1041.
Rajabi, M., Sherkati, S., Bohloli, B., Tingay, M., 2010. Subsurface fracture analysis and determination of in-situ stress direction using FMI logs: an example from the Santonian carbonates (Ilam Formation) in the Abadan Plain, Iran. Tectonophysics 492, 192–200. https://doi.org/10.1016/J.TECTO.2010.06.014.
Rajabi, M., Tingay, M., Heidbach, O., 2016. The present-day state of tectonic stress in the Darling Basin, Australia: implications for exploration and production. Mar. Petrol. Geol. 77, 776–790. https://doi.org/10.1016/J.MARPETGEO.2016.07.021.
Ramsay, J.G., 1980. The crack-seal mechanism of rock deformation. Nature 284, 135–139. https://doi.org/10.1038/284135a0.
Renard, F., Andréani, M., Boullier, A.Mi., Labaume, P., 2005. Crack-seal patterns: records of uncorrelated stress release variations in crustal rocks. Geol. Soc. Spec. Publ. 243, 67–79. https://doi.org/10.1144/GSL.SP.2005.243.01.07.
Rybacki, E., Meier, T., Dresen, G., 2016. What controls the mechanical properties of shale rocks? - Part II: Brittleness. J. Pet. Sci. Eng. 144, 39–58. https://doi.org/10.1016/j.petrol.2016.02.022.
Schmitt, D.R., Currie, C.A., Zhang, L., 2012. Crustal stress determination from boreholes and rock cores: fundamental principles. Tectonophysics 580, 1–26. https://doi.org/10.1016/J.TECTO.2012.08.029.
Shan, C., 2020. Study on Shale Gas Accumulation Conditions of the Lower Cambrian Niutitang Formation in the Micangshan Area.
Stevens, P., 2012. The 'Shale Gas Revolution': Developments and Changes. Chatham House Brief. Pap. 12.
Sverjensky, D.A., 1984. Europium redox equilibria in aqueous solution. Earth Planet Sci. Lett. 67, 70–78. https://doi.org/10.1016/0012-821X(84)90039-6.
Teixeira, M.G., Donzé, F., Renard, F., Panahi, H., Papachristos, E., Scholtès, L., 2017. Microfracturing during primary migration in shales. Tectonophysics 694, 268–279. https://doi.org/10.1016/J.TECTO.2016.11.010.
Tian, H., Zeng, L., Xu, X., Li, H., Luo, B., Dong, S., 2021. Factors influencing the in-situ stress orientations in shales: A case study of the Wufeng-Longmaxi formations in the Jiaoshiba Area, southeastern Sichuan Basin, China. J. Nat. Gas Sci. Eng. 94. https://doi.org/10.1016/j.jngse.2021.104110.
Tian, H., Zeng, L., Xu, X., Shu, Z., Peng, Y., Mao, Z., Luo, B., 2020. Characteristics of natural fractures in marine shale in Fuling area, Sichuan Basin, and their influence on shale gas. Oil Gas Geol. 41 (3), 474–483. https://doi.org/10.11743/ogg20200304.
Tingay, M.R.P., Morley, C.K., Hillis, R.R., Meyer, J., 2010. Present-day stress orientation in Thailand's basins. J. Struct. Geol. 32, 235–248. https://doi.org/10.1016/J.JSG.2009.11.008.
Uysal, I.T., Feng, Y. xing, Zhao, J. xin, Bolhar, R., Işik, V., Baublys, K.A., Yago, A., Golding, S.D., 2011. Seismic cycles recorded in late Quaternary calcite veins: geochronological, geochemical and microstructural evidence. Earth Planet Sci. Lett. 303, 84–96. https://doi.org/10.1016/j.epsl.2010.12.039.
Wagner, T., Boyce, A.J., Erzinger, J., 2010. Fluid-rock interaction during formation of metamorphic quartz veins: a REE and stable isotope study from the Rhenish Massif, Germany. Am. J. Sci. 310, 645–682. https://doi.org/10.2475/07.2010.04.
Wang, Q., Chen, X., Jha, A.N., Rogers, H., 2014. Natural gas from shale formation – the evolution, evidences and challenges of shale gas revolution in United States. Renew. Sustain. Energy Rev. 30, 1–28. https://doi.org/10.1016/J.RSER.2013.08.065.
Wang, Z., 2014. Practice and cognition of shale gas horizontal well fracturing stimulation in Jiaoshiba of Fuling area. Oil Gas Geol. 35, 425–430. https://doi.org/10.11743/ogg201418.
Watson, E.B., 2004. A conceptual model for near-surface kinetic controls on the trace-element and stable isotope composition of abiogenic calcite crystals. Geochem. Cosmochim. Acta 68, 1473–1488. https://doi.org/10.1016/J.GCA.2003.10.003.
Williams, J.D.O., Fellgett, M.W., Kingdon, A., Williamson, J.P., 2015. In-situ stress orientations in the UK Southern North Sea: regional trends, deviations and detachment of the post-Zechstein stress field. Mar. Petrol. Geol. 67, 769–784. https://doi.org/10.1016/J.MARPETGEO.2015.06.008.
Xu, X., Zeng, L., Tian, H., Ling, K., Che, S., Yu, X., Shu, Z., Dong, S., 2021. Controlling factors of lamellation fractures in marine shales: a case study of the Fuling Area in Eastern Sichuan Basin, China. J. Pet. Sci. Eng. https://doi.org/10.1016/j.petrol.2021.109091.
Zeng, L., Lyu, W., Li, J., Zhu, L., Weng, J., Yue, F., Zu, K., 2016. Natural fractures and their influence on shale gas enrichment in Sichuan Basin, China. J. Nat. Gas Sci. Eng. 30, 1–9. https://doi.org/10.1016/j.jngse.2015.11.048.
Zeng, W., Zhang, J., Ding, W., Zhao, S., Zhang, Y., Liu, Z., Jiu, K., 2013. Fracture development in Paleozoic shale of Chongqing area (South China). Part one: fracture characteristics and comparative analysis of main controlling factors. J. Asian Earth Sci. 75, 251–266. https://doi.org/10.1016/j.jseaes.2013.07.014.
Zhang, Y., He, Z., Jiang, S., Lu, S., Xiao, D., Chen, G., Li, Y., 2019. Fracture types in the lower Cambrian shale and their effect on shale gas accumulation, Upper Yangtze.

Mar. Petrol. Geol. 99, 282–291. https://doi.org/10.1016/J.MARPETGEO.2018.10.030.
Zhang, Y., Wei, S., Li, J., Wang, R., Li, H., Dong, S., 2010. Formation mechanism of the dabashan foreland arc-shaped structural belt. Acta Geol. Sin. 84, 1300–1313.
Zhao, J., Jin, Z., Lin, C., Liu, G., Liu, K., Liu, Z., Zhang, Y., 2019. Sedimentary environment of the lower Cambrian Qiongzhusi formation shale in the upper Yangtze region. Oil Gas Geol. 40, 701–715. https://doi.org/10.11743/ogg20190402.
Zhu, W., Dengfa, H., Chun, F., Zheng, M., 2013. Analysis of the multi-detachment structure in Micangshan Thrust belt, northern Sichuan Basin. Xinjiang Pet. Geol. 34, 282–286.
Zoback, M.D., Barton, C.A., Brudy, M., Castillo, D.A., Finkbeiner, T., Grollimund, B.R., Moos, D.B., Peska, P., Ward, C.D., Wiprut, D.J., 2003. Determination of stress orientation and magnitude in deep wells. Int. J. Rock Mech. Min. Sci. 40, 1049–1076. https://doi.org/10.1016/J.IJRMMS.2003.07.001.
Zou, C., Zhao, Q., Cong, L., Wang, H., Shi, Z., Wu, J., Pan, S., 2021. Development progress, potential and prospect of shale gas in China. Nat. Gas. Ind. 41, 1–14. https://doi.org/10.3787/j.issn.1000-0976.2021.01.001.